Surface-enhanced second-harmonic diffraction: Selective enhancement by spatial harmonics

Andrew C. R. Pipino, George C. Schatz, and Richard P. Van Duyne
Department of Chemistry, Northwestern University, 2145 Sheridan Road, Evanston, Illinois 60208
(Received 18 October 1993)

Surface-enhanced second-harmonic diffraction from a corrugated silver surface is studied as a function of the Fourier decomposition of the surface profile. Numerical results are obtained using the reduced Rayleigh equations for the linear and second-harmonic fields. Scattering of the surface-plasmon-polariton (SPP) -enhanced, evanescent nonlinear polarization wave into radiative channels is shown to provide a sensitive probe of spatial-harmonic content. The presence of a specific higher harmonic in the surface profile allows preferential scattering of the enhanced nonlinear polarization into a certain diffraction order where a higher-order scattering mechanism might otherwise be operative. The propagating orders can thereby be selectively enhanced, in some cases, by many orders of magnitude. Calculations are presented for symmetric profiles and a range of grating periods. The nature of these selective enhancements suggests that optimized profiles for second-harmonic diffraction into a particular order can be formed by a superposition of two appropriately selected Fourier components. To explore this possibility, gratings with groove densities of 1200 and 1290 grooves/mm were studied by first determining the enhancement of each of the propagating orders at their respective optimum groove depths, assuming a purely sinusoidal profile. A search for the maximum enhancement of each order was then performed by varying the amplitudes of the grating fundamental and relevant order-enhancing higher harmonic. For the two periods considered, optimized profiles were found. The degree of coupling to the SPP at the second-harmonic frequency is shown to be important in determining the optimized profile as demonstrated by the substantially different enhancing properties of these similar groove-density gratings.

INTRODUCTION

The study of surface-plasma wave resonances has a long and rich history. The associated effects, which appear in certain diffraction grating spectra, were originally observed by Wood[1] in 1902. Fano[2] later explained these diffraction anomalies by invoking the existence of a surface excitation for metals now known as the surface-plasmon polariton (SPP).[3] These excitations are slow, transverse magnetic-surface electromagnetic waves which have maximum amplitude at the metal-dielectric interface and decay exponentially away from the boundary. Interaction of electromagnetic radiation with the SPP mode occurs only through diffractive coupling or by phase matching with the attenuated total-reflectance (ATR) configuration.[4] In recent years, the study of SPP resonances has been reinvigorated by the discovery of surface-enhanced spectroscopy[5–7] including surface-enhanced Raman scattering[8] (SERS) and surface-enhanced second-harmonic generation (SESHG),[9] since this excitation is known to play a major role in the enhancement mechanism. Fundamental studies of SERS and SESHG have typically focused on quantitative analysis of the effect and on understanding the surface morphology and frequency dependence of these phenomena. In the case of SERS, to achieve the maximum electromagnetic enhancement[10] of 10^4–10^5 requires maximum enhancement at both the fundamental and Raman-shifted frequencies.[6] Although early studies of SERS on gratings[11–16] were critical for identifying the contribution ($\sim 10^2$) to the total enhancement due to amplification of the incident field by diffractive coupling to the SPP, the maximum enhancement at the Raman-shifted frequency cannot be achieved for normal Raman spectroscopy on gratings due in part to the incoherent nature of the Raman-scattering mechanism.[17] Experimental studies of SERS have shown that the largest enhancements are obtained on randomly roughened surfaces[8] or particle arrays,[7] where localized plasmons can be efficiently excited at both the incident and Raman-shifted frequencies. In contrast to SERS, SESHG involves a *coherent* three-photon process, which should allow optimization of enhancement via extended plasmons at both the fundamental and second-harmonic frequencies on a periodic surface. Indeed, both calculations and experiments have revealed that SHG enhancement on gratings can equal or exceed enhancement on randomly rough surfaces.[9,18–24]

The magnitude of SHG enhancement obtained from gratings is dependent on grating period, profile, and diffraction order, as these factors determine the efficiency of scattering of the localized SPP-enhanced second-harmonic fields into the propagating orders as well as the extent of SPP coupling at the fundamental and second-harmonic frequencies. Scattering efficiency of the localized field into the propagating orders increases with increasing grating period due to the smaller momentum transfer required.[21] Furthermore, the presence of higher Fourier components in the surface profile should strongly affect the distribution of intensity in the propagating orders in a manner similar to that which arises in linear diffraction under first-order SPP coupling conditions, as discussed by Rosengart and Pockrand.[25] Yet, the profile dependence of second-harmonic diffraction has only been

briefly explored theoretically by Reinisch *et al.*[22] For the triangular and trapezoidal profiles they considered, a strong dependence was found but the detailed physics was obscured by the complicated Fourier decomposition of these profile functions. In experiments where gratings are fabricated holographically, the profiles produced are nearly sinusoidal in many cases.[26,27] Under these conditions, the effect of higher harmonics on diffraction intensities has a simple interpretation and can be easily studied with a diffraction theory which is derived for a general profile function. Using the reduced Rayleigh equations for second-harmonic diffraction,[24] we show that, in the weak corrugation limit, SPP coupling provides a sensitive approach for probing the spatial-harmonic content of a nearly sinusoidal surface and a simple way to identify the optimized surface for second-harmonic diffraction into a particular order.

To provide credence concerning the predictive abilities of our choice of theory and motivation for our investigation of SESHG using second-harmonic-diffraction theory, the relevant literature will be briefly reviewed. Numerous theories for SESHG have been developed, including approaches that treat either localized plasmons using particle models[6,19,28] or extended plasmons using diffraction theories.[21,22,24,29–31] One important result from particle models is the prediction of an optimum particle size for local-field enhancement, which arises from a balance between radiation damping, dynamic depolarization, and electron mean-free-path effects in the excitation of localized plasmons. Similarly, rigorous linear diffraction theories,[14–16,32] which do not treat the roughness amplitude as a small parameter relative to the wavelength of light, predict an optimum corrugation depth for linear-field enhancement by photon-SPP coupling. Rigorous nonlinear diffraction theories[21,22,24,30,33] also show an optimum groove depth for second-harmonic diffraction, which has been observed experimentally.[20] Optimization of second-harmonic diffraction or linear-field enhancement typically occurs at surprisingly shallow groove depths.[14–16,20,22] Within this range of corrugation depths, the reduced Rayleigh equations are among the available nonperturbative methods for calculation of second-harmonic intensities,[24] although no SHG optimum groove-depth calculations have been reported previously using this method. We expect that for a theoretical study of SESHG, which is a process linked to the efficient excitation of the SPP, the capability of prediction of an optimum corrugation depth is crucial.

A second important aspect of theories of SESHG is the treatment of the nonlinear polarization including both surface and bulk contributions. For centrosymmetric materials, it is well known that SHG is dipole forbidden in the bulk, but that this restriction is removed in the presence of an interface due to breaking of the inversion symmetry.[34] The high surface sensitivity of the technique for centrosymmetric materials, which has been exploited in numerous applications,[35] originates from the dipole-allowed contribution arising from the layer of truncated unit cells present at the surface. For free-electron-like materials, which also show sharp and intense SPP resonances, the surface source of SHG can be described by two-induced second-harmonic-surface current densities of δ-function extent.[36] In the notation of Farias and Maradudin[24] and the coordinate system of Fig. 1, the parallel and perpendicular current densities are given by

$$J_x(\mathbf{x}|2\omega)=4(-2i\omega)\gamma b_s E_z(\mathbf{x}|\omega)E_x(\mathbf{x}|\omega)|_{z=0^-}\delta(z-0^+)\,, \tag{1a}$$

$$J_z(\mathbf{x}|2\omega)=2(-2i\omega)\gamma a_s E_z(\mathbf{x}|\omega)E_z(\mathbf{x}|\omega)|_{z=0^-}\delta(z-0^+) \tag{1b}$$

with

$$\gamma=\frac{e}{8m\omega^2}\frac{1-\epsilon(\omega)}{4\pi}\,,$$

where the E_i are the electric-field components, e and m are the electronic charge and mass, respectively, and $\epsilon(\omega)$ is the frequency-dependent dielectric function of the metal. Weaker bulk source terms of higher multipole character give rise to a bulk second-harmonic current, which originates from approximately a skin depth of material. This bulk nonlinear polarization $\mathbf{P}_B$, which can be expressed as[34,36,38]

$$\mathbf{P}_B(\mathbf{x}|2\omega)=\gamma\nabla[\mathbf{E}(\mathbf{x}|\omega)\cdot\mathbf{E}(\mathbf{x}|\omega)]\,, \tag{2}$$

produces a contribution to the total second-harmonic signal, which is typically of comparable magnitude to that generated by the surface currents.[30,37] The two phenomenological parameters in Eq. (1), a_s and b_s, were introduced by Rudnick and Stern[36] to account for variation of the perpendicular and parallel surface currents. The b_s parameter was expected to be frequency and material independent, but dependent on the surface profile with $b_s=-1$ or $-\frac{1}{2}$ for a flat or randomly rough surface, respectively. The a_s parameter, which was predicted to be frequency and material dependent, has been the subject of

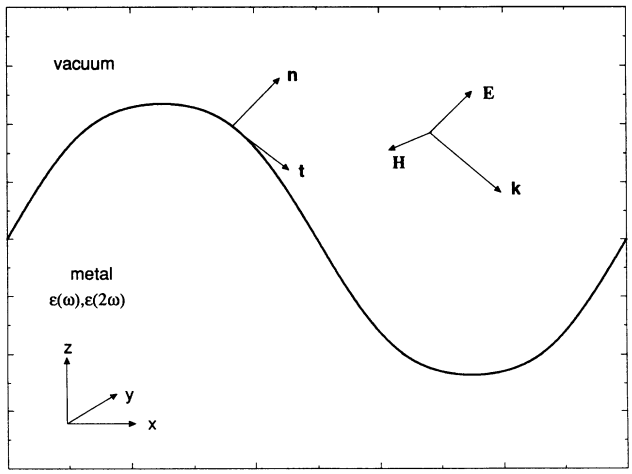

FIG. 1. A *p*-polarized plane wave with wave vector **k** is incident on a corrugated metal surface with dielectric functions $\epsilon(\omega),\epsilon(2\omega)$. The z axis is taken to be the grating normal.

numerous investigations.[38,39] Using the hydrodynamic model for the electron gas, Sipe *et al.*[38] reconsidered the problem of metal-surface SHG and found the same general form for the surface currents as well as expressions for the phenomenological parameters by assuming the thickness of the dipole-active region to be small relative to the wavelength. A fundamental assumption in the work of Rudnick and Stern[36] and Sipe *et al.*[38] was that the general expression originally derived by Bloembergen *et al.*[34] for the nonlinear polarization of an isotropic, centrosymmetric medium, given by

$$\mathbf{P}^{\mathrm{NL}}(2\omega)=(\delta-\beta-2\gamma)[\mathbf{E}(\omega)\cdot\nabla]\mathbf{E}(\omega)+\beta\mathbf{E}(\omega)[\nabla\cdot\mathbf{E}(\omega)] +\gamma\nabla[\mathbf{E}(\omega)\cdot\mathbf{E}(\omega)] , \quad (3)$$

where δ and β are material-dependent parameters, failed to hold at the metal surface. More recently, Maystre, Neviere, and Reinisch,[40] using the fact the Maxwell's equations are valid in the sense of distributions,[41] have reexamined Eq. (3) to find source terms of essentially identical form to those developed by Rudnick and Stern[36] but with no need for phenomenological parameters. However, in a comparison between theory and second-harmonic reflectivity measurements,[42] the introduction of two parameters into the theory of Maystre, Neviere, and Reinisch[40] was required to achieve a reasonable fit to the experimental data. The same values for these parameters were then successfully used to fit the results of surface-enhanced second-harmonic-diffraction experiments.[22] Similarly, using the reduced Rayleigh equations for second-harmonic diffraction[24] with the source terms of Sipe *et al.*,[38] Quail and Simon[23] obtained quantitative agreement between theory and measurements of several diffraction orders assuming $b_s=-1$ and using $a_s=+0.9$ for silver, as obtained from independent flat-surface measurements.[43] These results suggest that for weakly corrugated metal surfaces and with the use of two adjustable parameters, which characterize the flat-surface nonlinear response, rigorous second-harmonic-diffraction theories, which do not treat the grating amplitude as a perturbation, should be useful for making quantitative predictions with an accuracy comparable to nonperturbative linear theories. The accuracy of linear-diffraction theories is typically limited more by knowledge of the surface-dielectric function and surface profile than by any aspect of the theory itself.[41] When used properly within their radius of convergence, these theories which fully account for retardation effects are quantitative even under conditions where surface-plasmon-resonance interactions are important.

Second-harmonic-diffraction theory also provides a particularly lucid perspective on the SESHG enhancement process. When the incident photon is efficiently coupled to the SPP in first order, the outgoing, specularly reflected wave at the fundamental frequency is dramatically reduced in intensity and the majority of the incident-beam energy is channeled into a single evanescent order, which is momentum matched with the SPP mode.[14–16] Through the nonlinear polarization of the metal, an intense evanescent second-order polarization wave is then created.[33] The scattering of this nonlinear polarization then largely determines the intensity distribution in the available propagating orders. Clearly, first-order scattering processes should dominate the optical response. For a single-sinusoid profile, this ordinarily leads to the strongest enhancement in that diffraction order, which differs by only a single-grating wave vector from the evanescent nonlinear polarization. The presence of higher harmonics in the surface profile can redistribute intensity by providing first-order scattering channels into other propagating orders. Small contributions of a particular higher harmonic to the surface profile can thereby produce a dramatic and easily predictable enhancement of a specific diffraction order. Quail and Simon[23] observed this effect experimentally for a 1200 groove/mm holographically fabricated grating. They required the addition of a 3% contribution of the third spatial harmonic to their theoretical profile function in order to account for the large measured enhancement of the +1 second-harmonic-diffraction order. For the 1200 groove/mm pure sinusoidal grating, significant enhancement of the +1 order from SPP coupling at the fundamental frequency would otherwise have occurred only through a third-order process.

The nature of the frequency and profile dependence of SPP coupling at the second-harmonic frequency is also lucidly revealed by a diffraction theory approach to SESHG. At low frequencies, such as for CO_2 laser experiments, the dispersion relation is approximately linear. This allows a double resonance to occur, since the SPP-enhanced second-order polarization lies on the surface-plasmon-polariton dispersion relation (SPPDR) in the same branch as the fundamental resonance.[44] Furthermore, by finding simultaneous solutions of the diffractive coupling equations, given by

$$\pm\frac{\omega}{c}\left[\frac{\epsilon(\omega)}{1+\epsilon(\omega)}\right]^{1/2}=\frac{\omega}{c}\sin\theta+\left[\frac{2\pi}{a}\right]n , \quad n=\pm1,\pm2,\ldots , \quad (4a)$$

$$\pm\frac{2\omega}{c}\left[\frac{\epsilon(2\omega)}{1+\epsilon(2\omega)}\right]^{1/2}=\frac{2\omega}{c}\sin\theta+\left[\frac{2\pi}{a}\right]m , \quad m=\pm1,\pm2,\ldots , \quad (4b)$$

where θ is the angle of incidence and a is the grating period, approximate conditions can be found for a wide range of incident frequencies, which result in excitation of opposite branches of the SPPDR at the fundamental and second-harmonic frequencies.

The variety of conditions for SPP coupling, combined with optimum groove-depth effects and the influence of spatial harmonics, reveals a richness in the profile dependence for SESHG, which is largely unexplored. This paper examines two aspects of the profile dependence of SPP-enhanced second-harmonic diffraction from periodic structures of silver using the theory of Farias and Maradudin,[24] which is derived for a general-profile function: (i) the effect of higher spatial harmonics on the enhancement of diffraction orders as determined by the scattering of the SPP-enhanced evanescent nonlinear polarization

wave, and (ii) the identification of the optimized profile for enhancement of a particular diffraction order. Two grating periods are considered for this latter case, including one where coupling to SPP modes at both the fundamental and second-harmonic frequencies is especially strong.

THEORY

Application of the reduced Rayleigh equations[45] to second-harmonic diffraction using the source terms of Sipe *et al.*,[38] will be briefly reviewed.[24] As shown in Fig. 1, a *p*-polarized plane wave of frequency ω is assumed incident from vacuum on a periodic metal surface described by the profile function $\zeta(x)$, with the plane of incidence perpendicular to the grating grooves. The metal is assumed to have complex dielectric functions $\epsilon(\omega)$ and $\epsilon(2\omega)$ at the fundamental and second-harmonic frequencies, respectively. Since only a single nonzero component of the magnetic field exists for the *p*-polarized excitation geometry, only the scalar-wave equations for the y component of the magnetic field H_y at the fundamental and second-harmonic frequencies are required. For the linear fields,

$$\left[\frac{\partial^2}{\partial x^2}+\frac{\partial^2}{\partial z^2}+\frac{\omega^2}{c^2}\right]H_y(x,z|\omega)=0, \quad z>\zeta(x)\ , \tag{5a}$$

$$\left[\frac{\partial^2}{\partial x^2}+\frac{\partial^2}{\partial z^2}+\frac{\omega^2\epsilon(\omega)}{c^2}\right]H_y(x,z|\omega)=0, \quad z<\zeta(x)\ . \tag{5b}$$

The magnetic field above and below the selvedge region can be expanded in reflected and transmitted amplitudes, A_p and B_p, respectively, according to

$$H_y(x,z|\omega)=\begin{cases} e^{ikx-i\alpha_0(k|\omega)z}+\sum_{p=-\infty}^{\infty}A_p(k|\omega)e^{ik_px+i\alpha_p(k|\omega)z}, & z>\zeta_{\max} \\ \sum_{p=-\infty}^{\infty}B_p(k|\omega)e^{ik_px-i\beta_p(k|\omega)z}, & z<\zeta_{\min} \end{cases} \tag{6}$$

with

$$\alpha_p(k|\omega)=\begin{cases}[(\omega^2/c^2)-k_p^2]^{1/2}, & k_p^2<\omega^2/c^2 \\ i[k_p^2-(\omega^2/c^2)]^{1/2}, & k_p^2>\omega^2/c^2\ ,\end{cases} \tag{7a}$$

$$\beta_p(k|\omega)=\left[\epsilon(\omega)\frac{\omega^2}{c^2}-k_p^2\right]^{1/2}, \quad \mathrm{Re}\beta_p>0, \quad \mathrm{Im}\beta_p>0\ , \tag{7b}$$

$$k_p=k+\frac{2\pi p}{a}=\frac{\omega}{c}\sin\theta+\frac{2\pi p}{a}, \quad p=0,\pm1,\pm2,\ldots\ . \tag{7c}$$

Assuming the Rayleigh hypothesis[46,47] to be valid, the magnetic field satisfies the usual boundary conditions of continuity for the tangential electric and magnetic-field components.[48] Expressed in terms of the magnetic field, the boundary conditions in the $(\hat{t},\hat{y},\hat{n})$ coordinate system where $\hat{n}$ and $\hat{t}$ are the unit vectors normal and tangential to the surface, respectively, become

$$H_y(x,z|\omega)|_{z=\zeta(x)^-}=H_y(x,z|\omega)|_{z=\zeta(x)^+} \tag{8a}$$

and

$$\frac{1}{\epsilon(\omega)}\frac{\partial}{\partial n}H_y(x,z|\omega)|_{z=\zeta(x)^-}=\frac{\partial}{\partial n}H_y(x,z|\omega)|_{z=\zeta(x)^+}\ , \tag{8b}$$

where $\partial/\partial n$ is the derivative along the normal to the interface. Substitution of Eq. (6) into the boundary conditions (8) yields two infinite sets of coupled linear equations for the linear reflected and refracted amplitudes, including evanescent orders. The transformation of Toigo *et al.*[45] yields the reduced Rayleigh equations for the refracted amplitudes,

$$\sum_{p=-\infty}^{\infty}\frac{\alpha_r(k|\omega)\beta_p(k|\omega)+k_rk_p}{\alpha_r(k|\omega)-\beta_p(k|\omega)}Y_{r-p}(\alpha_r,\beta_p)B_p(k|\omega)=\frac{2\epsilon(\omega)\alpha_0}{1-\epsilon(\omega)}\delta_{r0}\ , \tag{9}$$

where

$$Y_{r-p}(\alpha_r,\beta_p)=\frac{1}{a}\int_{-a/2}^{+a/2}dx\,\exp\{-i(k_r-k_p)x+i[\alpha_r-\beta_p]\zeta(x)\}\ . \tag{10}$$

Only the refracted amplitudes are needed to solve the nonlinear problem since it is the field inside the metal that determines the nonlinear polarization.[38] Furthermore, because the bulk nonlinear polarization of the electron gas can be expressed as the gradient of a scalar function [see Eq. (2)], the wave equation for the second-harmonic field in the metal is homogeneous. The nonlinear polarization then enters into the problem only through inhomogeneous boundary conditions. Hence, the wave equation for the nonlinear problem can be written as

$$\left[\frac{\partial^2}{\partial x^2}+\frac{\partial^2}{\partial z^2}+\frac{4\omega^2}{c^2}\right]H_y(x,z|2\omega)=0, \quad z>\zeta(x)\ , \tag{11a}$$

$$\left[\frac{\partial^2}{\partial x^2}+\frac{\partial^2}{\partial z^2}+\frac{4\omega^2\epsilon(2\omega)}{c^2}\right]H_y(x,z|2\omega)=0, \quad z<\zeta(x)\ . \tag{11b}$$

The fields are again expanded in diffracted amplitudes according to

$$H_y(x,z|2\omega)=\begin{cases}\sum_{p=-\infty}^{\infty} A_p(2k|2\omega)e^{ik_p(2k|2\omega)x+i\alpha_p(2k|2\omega)z}, & z>\zeta_{\max}\\ \sum_{p=-\infty}^{\infty} B_p(2k|2\omega)e^{ik_p(2k|2\omega)x-i\beta_p(2k|2\omega)z}, & z<\zeta_{\min}\end{cases} \tag{12}$$

with

$$\alpha_p(2k|2\omega)=\begin{cases}[(4\omega^2/c^2)-[k_p(2k|2\omega)]^2]^{1/2}, & [k_p(2k|2\omega)]^2<4\omega^2/c^2\\ i[(k_p(2k|2\omega)]^2-(4\omega^2/c^2)]^{1/2}, & [k_p(2k|2\omega)]^2>4\omega^2/c^2\end{cases}, \tag{13a}$$

$$\beta_p(2k|2\omega)=\left[\epsilon(2\omega)\frac{4\omega^2}{c^2}-[k_p(2k|2\omega)]^2\right]^{1/2}, \quad \mathrm{Re}\beta_p(2k|2\omega)>0, \quad \mathrm{Im}\beta_p(2k|2\omega)>0, \tag{13b}$$

$$k_p(2k|2\omega)=2k+\frac{2\pi p}{a}=\frac{2\omega}{c}\sin\theta+\frac{2\pi p}{a}, \quad p=0,\pm1,\pm2,\ldots. \tag{13c}$$

The parallel and perpendicular source terms given by Eqs. (1a) and (1b) give rise to a parallel surface current and surface-dipole moment density, respectively. For a planar metal surface, the inhomogeneous boundary conditions are

$$\hat{z}\times\mathbf{H}(\mathbf{x}|2\omega)|\pm = \left[\frac{4\pi}{c}(-2i\omega)[4\gamma b_s E_z(\mathbf{x}|\omega)][E_x(\mathbf{x}|\omega)]|_{z=0^-}\right]\hat{x} \tag{14a}$$

and

$$\hat{x}\cdot\mathbf{E}(\mathbf{x}|2\omega)|\pm=4\pi\{\nabla[2\gamma a_s E_z(\mathbf{x}|\omega)E_z(\mathbf{x}|\omega)]|_{z=0}\}\cdot\hat{x}\ . \tag{14b}$$

If it is assumed that the phenomenological parameters a_s and b_s are not affected by the slowly varying corrugation, then the source terms can be used to determine the boundary conditions at the corrugated surface by making the transformation to the $(\hat{t},\hat{y},\hat{n})$ coordinate system in Eqs. (14). After expressing the corrugated boundary conditions entirely in terms of the magnetic fields, substitution of Eq. (12) into the boundary conditions yields two infinite sets of coupled linear equations for the second-harmonic reflected and refracted amplitudes. Again, using the transformation of Toigo *et al.*,[45] the reduced Rayleigh equations for the second-harmonic reflected amplitudes, which are of similar form to Eq. (9) and depend on the linear-diffraction amplitudes, are obtained. These equations include coupling to all orders. This approach is intermediate in rigor between perturbation theories,[29,31] which only include coupling to a particular order and the approach of Reinisch and Neviere,[33] which uses an additional expansion for the fields in the selvedge region. Equation (9) and its nonlinear analog are solved by increasing the number of diffraction amplitudes in the expansion until a preset convergence level is achieved. The integrals (10) and those that arise in the nonlinear theory are evaluated using a Gaussian quadrature scheme.[49] Our calculations agree quantitatively with the results of Quail and Simon[23] using the dielectric functions of Dujardin and Theye.[50]

The convergence properties of diffraction theories based on the Rayleigh hypothesis are still a subject of active investigation.[46] Convergence is frequently discussed in terms of the ratio of grating amplitude-to-period, ζ_0/a, without regard to the ratio of period-to-wavelength. At least for linear diffraction, a recent investigation by Paulick[46] gives $\zeta_0/a\leq 0.0713$ as the upper bound for the validity of the Rayleigh hypothesis, with previous investigations[47,51] suggesting $\zeta_0/a\approx 0.1$ as an upper bound. For surfaces formed from simple superpositions, the Rayleigh hypothesis is valid but the radius of convergence is limited by the effective ζ_0/a for the highest-frequency component in the superposition.[52] For profile functions expressed as an infinite Fourier series, the Rayleigh hypothesis is theoretically never valid.[52] However, the theoretical limit for application of the Rayleigh method is not necessarily meaningful in practice since, as Wirgin points out,[53] a divergent result can be obtained at any amplitude-to-period ratio by including too many terms in the Fourier expansion for the fields. Furthermore, useful results can be obtained for values of ζ_0/a which exceed the theoretical upper bound by using a severely truncated expansion.[54,55] These effects likely result from use of a complete but nonorthogonal set of functions[45] and/or the numerical instabilities in the phase factors at large orders.[51] The convergence properties of the reduced Rayleigh equations for second-harmonic generation have not specifically been explored. It is worth noting that this treatment of second-harmonic diffraction does not account for SPP self-phase modulation or Gaussian beam-dependent effects,[56,57] which may be encountered in experiments.

RESULTS AND DISCUSSION

Selective enhancement of diffraction orders

To study the effect of the spatial harmonics on the propagating second-harmonic-diffraction orders, periods ranging from 0.8 to 1.6 μm in increments of 0.2, with even profiles, were considered. Beyond the 1.0-μm case,

each period allows one additional propagating second-harmonic order under first-order SPP coupling at the incident frequency. This allows the next higher spatial harmonic to interact with a propagating order and thereby to be probed experimentally. All angles of incidence are chosen as positive for these symmetric profiles, which leads to positive first-order coupling for periods above 1.0 μm and negative first-order coupling otherwise. The enhancement of the nth diffraction order is defined relative to the planar surface response at the same angle of incidence according to

$$I_n = \frac{\alpha_n(2k|2\omega)|A_n(2k|2\omega)|^2}{\alpha_0(2k|2\omega)|A_f(2k|2\omega)|^2}, \tag{15}$$

where A_f is the planar surface-reflected amplitude.[24,38] Table I shows the change in enhancement, relative to the pure sinusoidal profile case, for all of the propagating orders which exist for each period considered, as a function of the higher harmonic amplitude for the second through sixth harmonics. Figures 2(a), 3(a), and 4(a) depict the influence of the second, third, and fourth spatial harmonics on the enhancement of the most strongly affected diffraction order in each case. Figures 2(b), 3(b), and 4(b) show the corresponding photon-plasmon coupling (PPC) diagrams. Within the range of grating amplitudes which optimize photon-SPP coupling at the fundamental frequency, the SPPDR for a flat surface can be used to interpret the selective enhancements. In the PPC diagrams, the normalized planar SPPDR, derived using the free-electron-gas dielectric constant and given by[4]

$$\frac{k_\parallel}{k_p} = \frac{\omega}{\omega_p}\left[\frac{1-(\omega_p/\omega)^2}{2-(\omega_p/\omega)^2}\right]^{1/2}, \tag{16}$$

where $k_p = \omega_p/c$ and ω_p is the bulk plasma frequency, is shown as the heavy solid line using ω_p for silver [9.04 eV (Ref. 28)]. The free-electron-gas dielectric constant, $\epsilon(\omega) = 1-(\omega_p/\omega)^2$, has been used only to generate the SPPDR curves for the purpose of illustration. All calculations assume an incident plane wave at 1.06 μm (1.17 eV) and use the dielectric functions of Dujardin and Theye.[50] The heavy dashed lines in the PPC diagrams form the light cone. All wave vectors lying outside this region correspond to evanescent waves. Within the light cone, the dotted lines describe the propagating diffraction orders which, by definition, differ from the specular order by an integer multiple of the fundamental grating wave vector. The SPPDR, which approaches the light line at low frequencies, describes a doubly degenerate surface excitation that can interact with electromagnetic radiation through surface roughness via an umklapp process.[4] In the PPC diagrams, arrows indicate an umklapp process in which either the incident wave is coupled to the SPP mode or the SPP-enhanced nonlinear polarization wave is scattered into a radiative channel at the second-harmonic frequency. The diffraction-order enhancements shown in Figs. 2(a), 3(a), and 4(a) were determined by varying the amplitude of a particular spatial harmonic, expressed as a fraction of the fundamental amplitude, with fixed $\zeta_0/a = 0.01$ for the fundamental.

The effect of a second spatial harmonic in the surface

TABLE I. The enhancement of diffraction orders, relative to the case of a pure sinusoidal profile, is shown for different values of the higher harmonic amplitudes. A high level of selectivity and sensitivity, which increase with harmonic order, is apparent.

Period (μm)	%	$\frac{I_{-4}(\%)}{I_{-4}(0)}$	$\frac{I_{-3}(\%)}{I_{-3}(0)}$	$\frac{I_{-2}(\%)}{I_{-2}(0)}$	$\frac{I_{-1}(\%)}{I_{-1}(0)}$	$\frac{I_0(\%)}{I_0(0)}$	$\frac{I_{+1}(\%)}{I_{+1}(0)}$
0.8000	0				1	1	1
second	2				0.998	1.58	1.06
Harmonic	5				0.994	3.62	1.20
	10				0.983	9.86	1.50
1.000	0				1	1	1
third	2				1.00	1.09	26.3
Harmonic	5				1.01	1.24	129
	10				1.01	1.52	467
1.2000	0			1	1	1	1
fourth	1			380	1.20	1.02	0.999
Harmonic	3			3416	1.80	1.06	0.997
1.4000	0		1	1	1	1	1
fifth	1		27 272	2.50	1.37	1	1
Harmonic	3		245 454	21.3	2.30	1.02	1
1.6000	0	1	1	1	1	1	1
sixth	1	9.42×10^6	600	2.4	1.23	1	1
Harmonic	3	6.3×10^7	12 500	4	1.33	1	1

profile on the specular SHG mode is shown in Fig. 2 for a grating period of 0.8 μm. The second-harmonic amplitudes are set equal to 0%, 2%, 5%, and 10% of the fundamental amplitude. The specular-order enhancement is seen to approximately triple with addition of a 5% contribution of the second spatial harmonic. The presence of this higher harmonic selectively enhances the specular SHG mode, while the other propagating orders are only slightly modified as shown in Table I. The PPC diagram provides an approximate interpretation. For conditions under which photon-SPP coupling occurs in first order at the fundamental frequency, the resulting intense second-order evanescent polarization wave is phase matched with the evanescent second diffraction order at the second-harmonic frequency. This SPP-enhanced second-order polarization wave is then selectively scattered into the specular SHG mode by the second spatial harmonic which provides a more probable first-order channel. Figure 3 shows the effect of a third spatial harmonic. In this case, the +1 SHG diffraction order is selectively enhanced, since the SPP-enhanced evanescent second-order polarization and the +1 SHG diffraction order are connected in first order by this spatial harmonic.[23] The sensitivity of the +1 order to the third harmonic is seen to be much greater than in the second harmonic case, since a 5% contribution gives rise to a several order-of-magnitude change in the enhancement. Figure 4 and Table I reveal the influence of the fourth, fifth, and sixth spatial harmonics, which selectively enhance the −2, −3, and −4 diffraction orders, respectively. The trend towards increased sensitivity for the higher harmonics is apparent. A 3% contribution of the sixth spatial harmonic gives rise to a nearly eight order-of-magnitude enhancement for the −4 diffraction order of the 625 groove/mm grating, relative to the case of a pure sinusoidal grating with the same period. Again as shown in the PPC diagrams, these selective enhancements occur by providing a first-order scattering channel for the SPP-enhanced second-order polarization wave into specific orders. The generality of this effect is predictable simply by combining the grating equations at the fundamental and second-harmonic frequencies under first-order photon-SPP coupling conditions at the fundamental frequency, with the phase-matching condition for the SPP-enhanced nonlinear polarization wave, which is well defined for weak corrugations. Note that in terms of

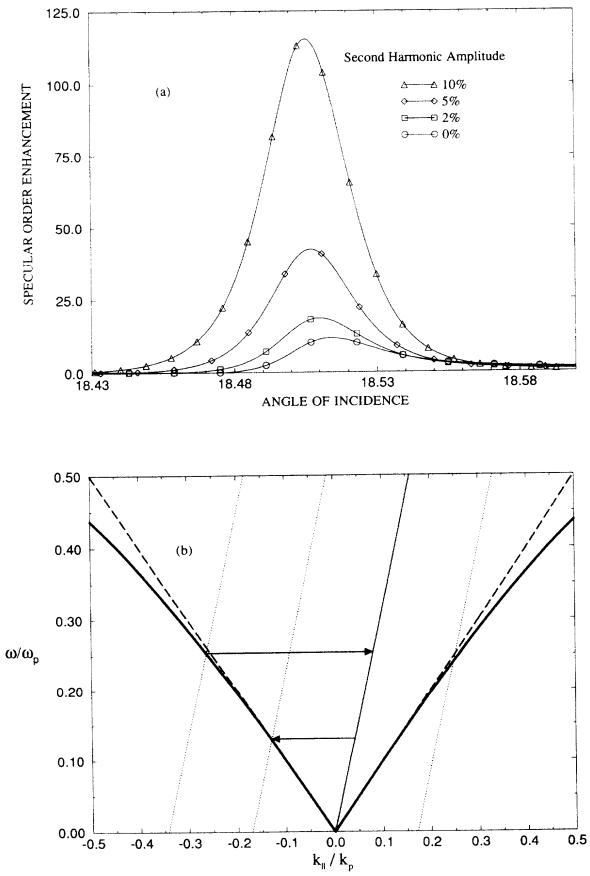

FIG. 2. Influence of the second spatial harmonic for a 0.8-μm period silver grating: (a) Intensity of the specular order vs angle of incidence θ (in degrees) for different second spatial-harmonic amplitudes. (b) The corresponding photon-plasmon coupling diagram.

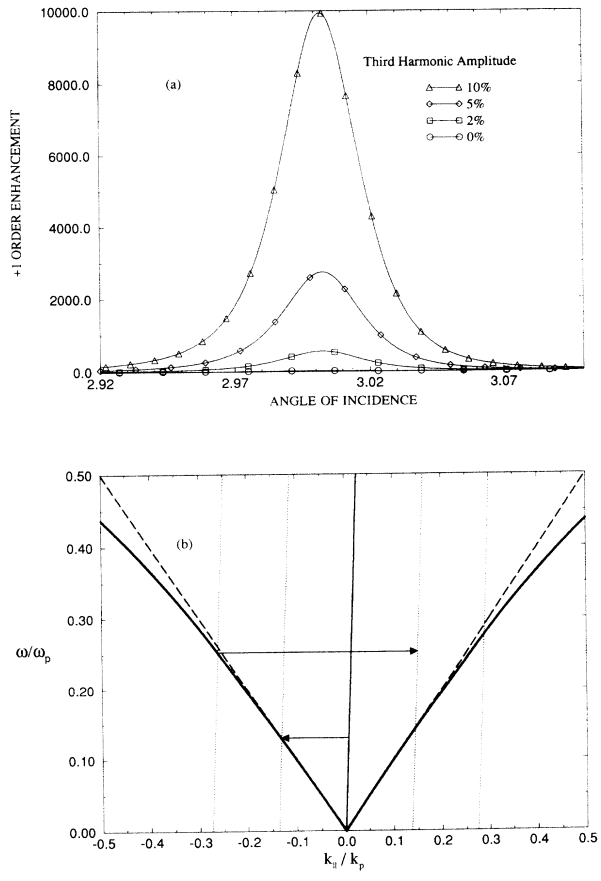

FIG. 3. Influence of the third spatial harmonic for a 1.0-μm silver grating: (a) Intensity of the +1 order vs θ (deg) for different third spatial-harmonic amplitudes. (b) The photon-plasmon coupling diagram.

absolute intensities these selective enhancements result in signals which are strong enough to be measurable[20,23] even for the higher spatial harmonics with amplitudes which are only 1% of the fundamental and which enhance otherwise very weak diffraction orders.

Optimized profiles

The nature of the selective enhancement of diffraction orders by spatial harmonics suggests that an optimized profile for second-harmonic diffraction into a particular order should exist. For a purely sinusoidal profile, the existence of an order-dependent optimum groove depth for second-harmonic diffraction is well established.[21,22,33] However, in considering a more general profile function the peak enhancement obtainable in a particular order is not necessarily expected to be limited by the peak enhancement achieved at the optimum groove depth for the corresponding sinusoidal profile. Depending upon the major source or sources for intensity in a particular order, the optimized profile should in general contain higher harmonics with optimized amplitudes, which directly connect intense evanescent orders with the propagating order being considered. To investigate this possibility, we examined the profile dependence of enhancement for gratings with groove densities of 1200 and 1290 grooves/mm, where in the second case coupling to the SPP at both the fundamental and second-harmonic frequencies is especially strong. We first find the optimum groove depths for the different propagating orders order of the purely sinusoidal profiles with these periods. The optimum amplitudes for the order-enhancing higher harmonics are then found for different fundamental amplitudes.

The existence of an optimum groove depth for second-harmonic diffraction is clearly related to the excitation of

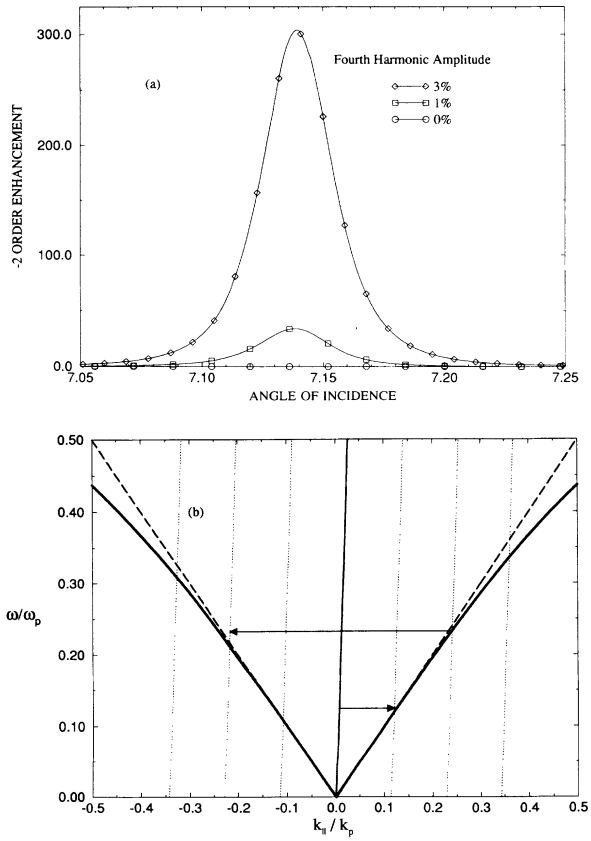

FIG. 4. Influence of the fourth spatial harmonic for a 1.2-μm silver grating: (a) Intensity of the -2 second-harmonic order vs θ (deg) for different fourth-harmonic amplitudes. (b) PPC diagram.

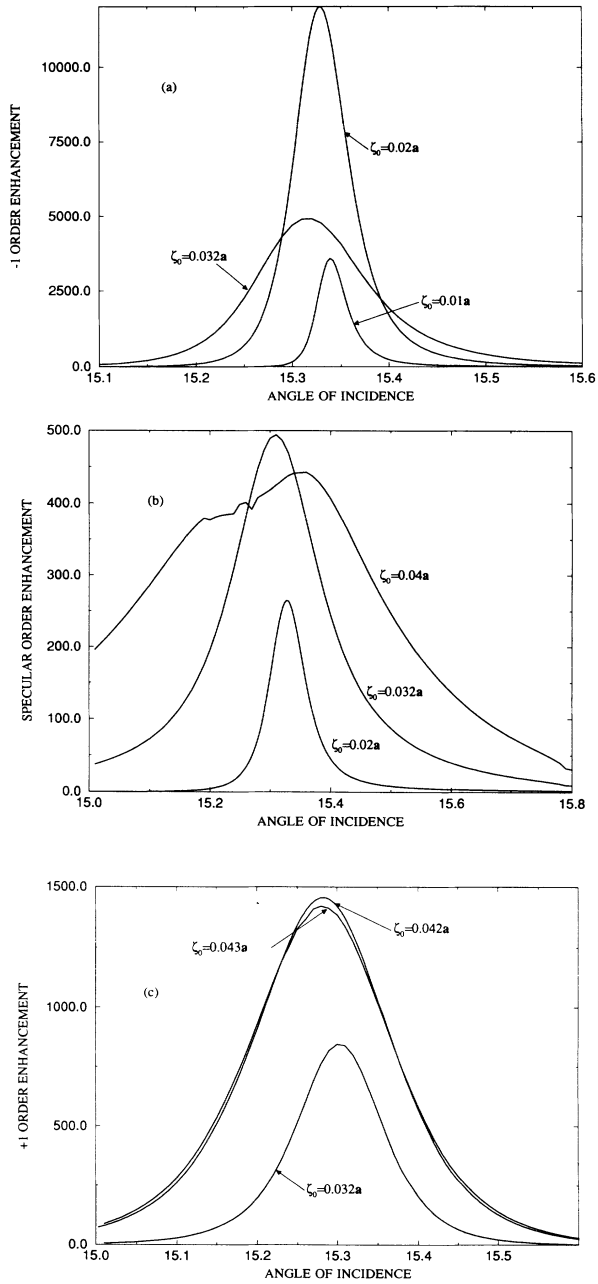

FIG. 5. Groove-depth dependence of the enhancement vs θ (deg) for the three propagating orders of a 1200-groove/mm grating: (a) -1 order (b) 0 order (c) $+1$ order.

the SPP at the fundamental frequency and corresponding field enhancement.[14–16] However, we find that the value of the groove depth which optimizes SHG is different from the value which produces the maximum field enhancement. Furthermore, the optimum groove depth typically increases for orders which differ increasingly in wave vector from the SPP-enhanced evanescent polarization wave. Although all of the diffraction order amplitudes are coupled at each frequency in the reduced Rayleigh method within an undepleted pump approximation, these trends can be analyzed by considering the major energy pathways. Figure 5 shows enhancement at different groove depths for the three propagating orders of a 1200-groove/mm pure sinusoidal grating of silver. For SPP coupling in the -1 linear diffraction order, enhancements are seen to optimize at approximately $\zeta_0/a=0.02$, 0.03, and 0.04 for the -1, 0, and $+1$ diffraction orders, respectively. With respect to the SPP-enhanced second-order polarization, enhancement of the -1, 0, and $+1$ SHG diffraction orders occurs through first-, second-, and third-order scattering processes, respectively. These processes become more favorable as the grating depth increases, in analogy with the radiation damping of the SPP.[58,59] The optimum groove depth for the -1 second-harmonic order arises from a competition between efficient excitation of the SPP at the fundamental frequency and scattering of the resulting evanescent second-order wave into this propagating order. The coupled process apparently optimizes at a slightly deeper groove than required for the maximum surface-field enhancement at the fundamental frequency. The surface field was found to maximize at $\zeta_0/a=0.016$, which also maximizes the evanescent second-order polarization-wave intensity. The existence of a deeper optimum depth for the 0 and $+1$ second-harmonic orders likely arises from the increased efficiency of second- and third-order scattering of the second-order polarization and from the spreading of energy at the fundamental frequency into other diffraction orders as the groove depth is increased. In particular, the 0 and $+1$ linear orders, which strongly affect the corresponding second harmonic orders, receive a rapidly increasing fraction of the total diffracted energy for groove depths beyond which the SPP wave becomes damped. As the groove depth is increased further, the fraction of energy in these orders eventually declines as higher orders receive an increasing share of the total. In the presence of two or more intense evanescent diffraction orders, the interaction between different orders through the nonlinear polarization could also be important.

The possibility of resonant excitation of the counter-propagating SPP at the second-harmonic frequency can influence the optimum groove depth and the peak enhancements at optimum as arises for the case of a 1290-grooves/mm grating. Figure 6 shows enhancement as a function of groove depth for the two propagating orders of this grating. In this case, the incident fundamental and outgoing second-harmonic specular orders both differ from the SPPDR by a single-grating wave vector. The 0 and -1 second-harmonic orders are seen to optimize at approximately $\zeta_0/a=0.02$ and 0.04, respectively, with the peak enhancement for the specular mode exceeding that of the -1 order by more than a factor of 2. In this special case, the propagating orders are reso-

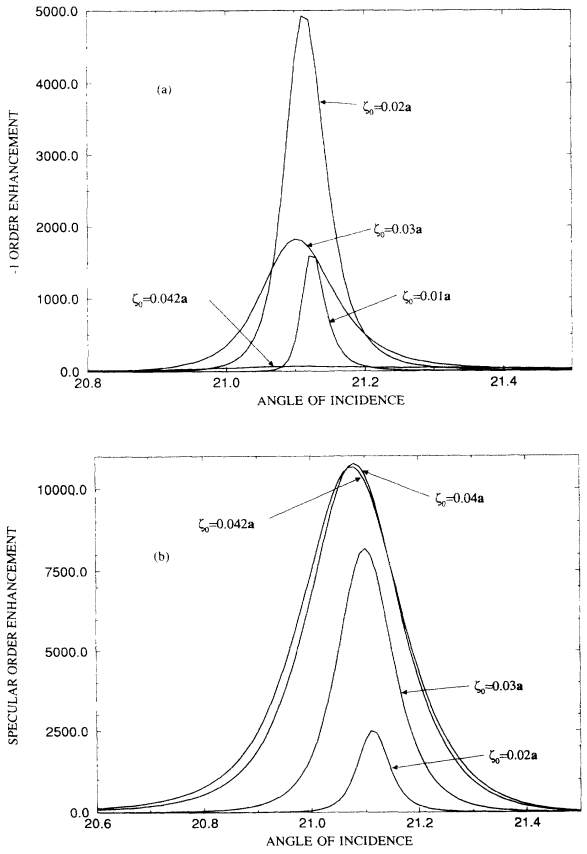

FIG. 6. Groove-depth dependence of the enhancement vs θ (deg) for the two propagating orders of a 1290-groove/mm grating: (a) -1 order (b) 0 order.

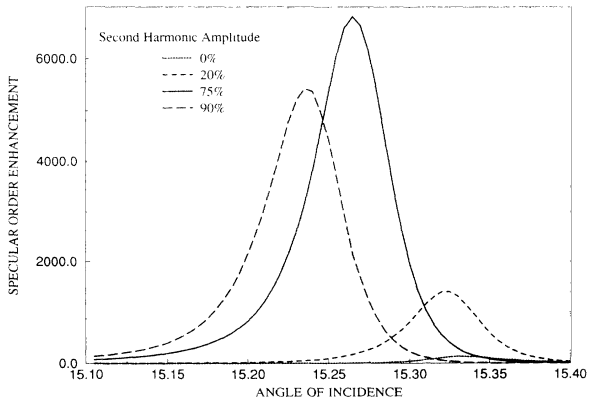

FIG. 7. Optimization of the specular SHG order vs θ (deg) for a 1200-groove/mm grating with $\zeta_0/a=0.016$. A 75% second-harmonic amplitude is shown to maximize SHG reflection in this case.

nantly enhanced through first- and second-order channels.

To find optimized profiles for second-harmonic diffraction in the weak corrugation limit, an optimum value for the amplitude of the higher spatial harmonic which connects the SPP-enhanced evanescent second-order polarization to the propagating order under consideration must be found. Since the -1 second-harmonic order differs by only one grating wave vector from the enhanced evanescent nonlinear polarization for the two gratings considered, a purely sinusoidal profile at the optimum groove depth will maximize enhancement for these orders. For the remaining orders, a two-Fourier-component optimized profile should exist. Figure 7 shows the enhancement of the specular order of the 1200-groove/mm grating for 0%, 20%, 75%, and 90% contributions of the second spatial harmonic for a fundamental amplitude of $\zeta_0/a=0.016$, which optimizes the magnitude of the evanescent nonlinear polarization. The specular order is seen to maximize at a very strong second-harmonic amplitude of 75% with the peak intensity exceeding that of the specular order at the optimum groove depth for a single sinusoidal grating by approximately a factor of 14. Slightly larger enhancements were obtained by slightly reducing the magnitude of the fundamental and increasing the second-harmonic amplitude. For this grating period, the effect of the second spatial harmonic on the specular order was also examined at the pure sinusoidal optimum groove depth of $\zeta_0/a=0.032$, but no significant enhancement over the sinusoidal case was found. Enhancement of the $+1$ order was also examined as a function of the third-harmonic amplitude. For $\zeta_0/a=0.016$, enhancements significantly exceeding the optimized pure sinusoidal case were found but no optimum third-harmonic amplitude was obtained in this case, although for $\zeta_0/a=0.02$ an optimum third-harmonic amplitude of 30% was found. For the 1290-groove/mm grating, which only allows two propagating orders, Fig. 8 shows the effect of the second spatial harmonic on the specular SHG mode for $\zeta_0/a=0.016$ and 0.04. An optimum is found in each case but the overall contribution of the higher harmonic to the enhancement is relatively small. The maximum enhancement obtained is very near that of the pure sinusoidal case since the optimum is largely controlled by the SPP resonance at the second-harmonic frequency in the evanescent $+1$ diffraction order. In this particular case, the optimized profile for second-harmonic reflection is essentially the sinusoidal profile.

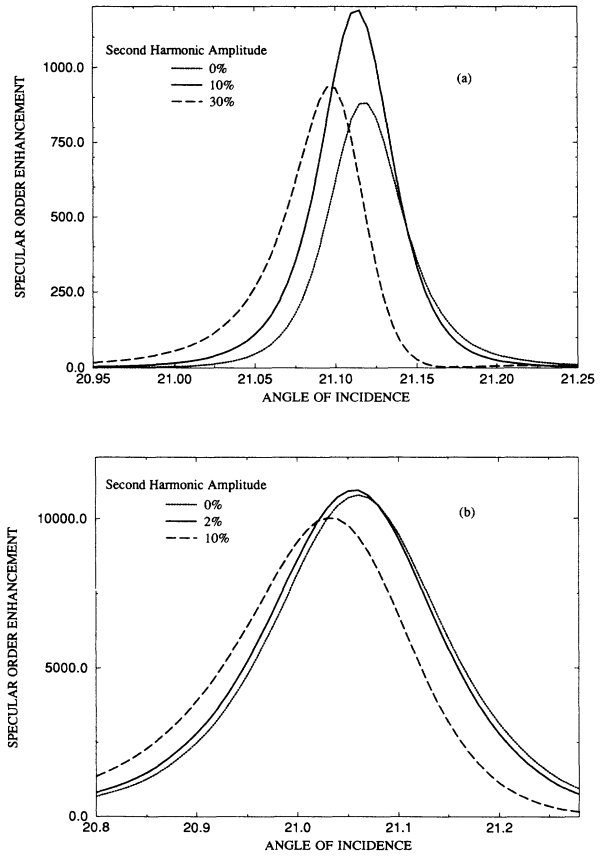

FIG. 8. Optimization of the specular SHG order vs θ (deg) for a 1290-groove/mm grating with (a) $\zeta_0/a=0.016$ and (b) $\zeta_0/a=0.04$. The effect of the second harmonic is relatively insignificant for this groove density.

CONCLUSION

The profile dependence of surface-enhanced second-harmonic diffraction has been explored using the reduced Rayleigh equations as originally developed by Farias and Maradudin.[24] The presence of weak spatial harmonics in the surface profile is found to selectively enhance specific diffraction orders in an easily predictable way, demonstrating the generality of the experimental observation of Quail and Simon.[23] Under conditions where the incident photon couples to the SPP in first order, the enhanced evanescent nonlinear polarization wave, which is distinct for a narrow but important range of groove depths, is phase matched with a second diffraction order at the second-harmonic frequency. This relatively intense evanescent wave then differs from the available propagating orders by an integer multiple of the grating wave vector. The sensitivity of these selective enhancements to the magnitude of the spatial harmonic increases with harmonic order. In light of the quantitative accuracy of the theory,[23] this method should provide a sensitive probe of profile quality for near sinusoidal profiles. Furthermore, the design of optimized profiles for second-harmonic diffraction with the potential for producing strong, second-harmonic beams, which are spatially separated from the fundamental reflection, appears feasible.

ACKNOWLEDGMENTS

This work was supported in part by the Donors of the Petroleum Research Fund of the American Chemical Society (Grant No. 24134-AC6) and in part by NSF Grant No. DMR-8802706.

[1]R. W. Wood, Philos. Mag. **4**, 396 (1902).
[2]U. Fano, J. Opt. Soc. Am. **31**, 213 (1941).
[3]*Surface Polaritons,* edited by V. M. Agranovich and D. L. Mills (North-Holland, Amsterdam, 1982).
[4]H. Raether, *Surface Plasmons on Smooth and Rough Surfaces and on Gratings,* Springer Tracts in Modern Physics Vol. 111 (Springer, Berlin, 1988).
[5]M. Moskovits, Rev. Mod. Phys. **57**, 783 (1985).
[6]G. C. Schatz, in *Fundamentals and Applications of Surface Raman Spectroscopy,* edited by R. L. Garrel, J. E. Pemberton, and T. M. Cotton (VCH, Deerfield Beach, FL, 1993).
[7]R. K. Chang and T. E. Furtak, *Surface Enhanced Raman Scattering* (Plenum, New York, 1982).
[8]M. Fleischman, P. J. Hendra, and A. J. McQuillan, Chem. Phys. Lett. **26**, 163 (1974); D. L. Jeanmaire and R. P. Van Duyne, J. Electroanal. Chem. **84**, 1 (1977).
[9]C. K. Chen, A. R. B. de Castro, and Y. R. Shen, Phys. Rev. Lett. B **46**, 145 (1981).
[10]Additional enhancement mechanisms have been proposed to account for a total enhancement of 10^6–10^7. See, for example, A. Otto, I. Mrozek, H. Grabhorn, and W. Akermann, J. Phys. Condens. Matter **4**, 1143 (1992).
[11]S. S. Jha, J. R. Kirtley, and J. C. Tsang, Phys. Rev. B **22**, 3973 (1980).
[12]J. C. Tsang, J. R. Kirtley, and T. N. Theis, Solid State Commun. **35**, 667 (1980).
[13]D. L. Mills and M. Weber, Phys. Rev. B **26**, 1075 (1982).
[14]M. Neviere and R. Reinisch, Phys. Rev. B **26**, 5403 (1982).
[15]N. Garcia, Opt. Commun. **45**, 307 (1983).
[16]N. Garcia, G. Diaz, J. J. Saenz, and C. Ocal, Surf. Sci. **143**, 342 (1984).
[17]M. Arnold, P. Bussemer, K. Hehl, H. Grabhorn, and A. Otto, J. Mod. Opt. **39**, 2329 (1992).
[18]A. Wokaun, J. G. Bergman, J. P. Heritage, A. M. Glass, P. F. Liao, and D. H. Olson, Phys. Rev. B **24**, 849 (1981).
[19]G. T. Boyd, Th. Rasing, J. R. R. Leite, and Y. R. Shen, Phys. Rev. B **30**, 519 (1984).
[20]J. L. Coutaz, D. Maystre, M. Neviere, and R. Reinisch, J. Appl. Phys. **62**, 1529 (1987).
[21]D. Maystre, M. Neviere, R. Reinisch, and J. L. Coutaz, J. Opt. Soc. **5**, 338 (1988).
[22]R. Reinisch, M. Neviere, H. Akhouayri, J. L. Coutaz, D. Maystre, and E. Pic, Opt. Eng. **27**, 961 (1988).
[23]J. C. Quail and H. J. Simon, J. Opt. Soc. Am. **5**, 325 (1988).
[24]G. A. Farias and A. A. Maradudin, Phys. Rev. B **30**, 3002 (1984).
[25]E.-H. Rosengart and I. Pockrand, Opt. Lett. **1**, 194 (1977).
[26]S. Austin and F. T. Stone, Appl. Opt. **15**, 1071 (1976).
[27]S. Austin and F. T. Stone, Appl. Opt. **15**, 2126 (1976).
[28]E. J. Zeman and G. C. Schatz, J. Phys. Chem. **91**, 634 (1987).
[29]G. S. Agarwal and S. S. Jha, Phys. Rev. B **26**, 482 (1982).
[30]M. Neviere, P. Vincent, D. Maystre, R. Reinisch, and J. L. Coutaz, J. Opt. Soc. Am. B **5**, 330 (1988).
[31]R. T. Deck and Grygier, Appl. Opt. **23**, 3202 (1984).
[32]A. A. Maradudin, J. Opt. Soc. Am. **73**, 759 (1983).
[33]R. Reinisch and M. Neviere, Phys. Rev. B **28**, 1870 (1983).
[34]N. Bloembergen, R. K. Chang, S. S. Jha, and C. H. Lee, Phys. Rev. **174**, 813 (1968).
[35]G. L. Richmond, J. M. Robinson, and V. L. Shannon, Prog. Surf. Sci. **28**, 1 (1988).
[36]J. Rudnick and E. A. Stern, Phys. Rev. B **4**, 4274 (1971).
[37]H. W. K. Tom, T. F. Heinz, and Y. R. Shen, Phys. Rev. Lett. **51**, 1983 (1983).
[38]J. E. Sipe, V. C. Y. So, M. Fukui, and G. I. Stegeman, Phys. Rev. B **21**, 4389 (1980).
[39]See, for example, W. L. Schaich and A. Liebsch, Phys. Rev. B **37**, 6187 (1988); M. G. Weber and A. Liebsch, *ibid.* **35**, 7411 (1987); A. Liebsch, Phys. Rev. Lett. **61**, 1233 (1988); R. Murphy, M. Yeganeh, K. J. Song, and E. W. Plummer, *ibid.* **63**, 318 (1989).
[40]D. Maystre, M. Neviere, and R. Reinisch, Appl. Phys. A **39**, 115 (1986).
[41]*Electromagnetic Theory of Gratings,* edited by R. Petit (Springer-Verlag, Berlin, 1980).
[42]J. L. Coutaz, D. Maystre, M. Neviere, and R. Reinisch, J. Appl. Phys. **62**, 1529 (1987).
[43]J. C. Quail and H. J. Simon, Phys. Rev. B **31**, 4900 (1985).
[44]D. L. Mills, Solid State Commun. **24**, 669 (1977).
[45]F. Toigo, A. Marvin, V. Celli, and N. R. Hill, Phys. Rev. B **15**, 5618 (1977).
[46]T. C. Paulick, Phys. Rev. B **42**, 2801 (1990).
[47]N. R. Hill and V. Celli, Phys. Rev. B **17**, 2478 (1978).
[48]J. D. Jackson, *Classical Electrodynamics* (Wiley, New York, 1975).
[49]W. H. Press, B. P. Flannery, S. A. Teukolsky, and W. T. Vetterling, *Numerical Recipes* (Cambridge University Press, New York, 1989).
[50]M. M. Dujardin and M. L. Theye, J. Phys. Chem. Solids **32**, 2033 (1971).
[51]D. Agassi and T. F. George, Phys. Rev. B **33**, 2393 (1986).
[52]P. M. Van den Berg and J. J. Fokkema, J. Opt. Soc. Am. **69**, 27 (1979).
[53]A. Wirgin, J. Opt. Soc. Am. **72**, 963 (1982).
[54]S. H. Zaidi, M. Yousaf, and S. R. J. Brueck, J. Opt. Soc. Am. B **8**, 770 (1991).
[55]S. H. Zaidi, M. Yousaf, and S. R. J. Brueck, J. Opt. Soc. Am. B **8**, 1348 (1991).
[56]G. Li and S. R. Seshadri, J. Opt. Soc. Am. B **7**, 998 (1990).
[57]G. Li and S. R. Seshadri, Phys. Rev. B **44**, 1240 (1991).
[58]N. E. Glass, M. Weber, and D. L. Mills, Phys. Rev. B **29**, 6548 (1984).
[59]M. G. Weber and D. L. Mills, Phys. Rev. B **31**, 2510 (1985).